Stretching the Design

M. Fernández-Barciela, A.M. Pelaez-Perez, S. Woodington, J.I. Alonso, and P.J. Tasker

In the design of most electronic circuits and systems, designers use computer-aided design (CAD) tools to guide the design flow. They exploit the ability of CAD tools to perform algebraic operations to compute/predict circuit and system performance. This is possible because, in most electronic circuits and systems, linear operation can be assumed. The behavior of microwave components, circuits, and systems can, for example, be described in terms of "behavioral" parameters, such as *Z*-parameters, *Y*-parameters, and *S*-parameters. Transformation from one parameter to another is achieved by simple linear algebraic operations [1]. The performance of more complex circuits can be computed via linear matrix operations using the relevant parameters, i.e., *Y*-parameters for parallel connections and *Z*-parameters for series connections. More significantly, performance predictions can also be obtained via linear algebra transformations, i.e., the maximum gain, minimum noise figure, potential instability, etc., along with design insight, i.e., gain circles, noise circles, optimum input/output match requirements, and so on [1], [2].

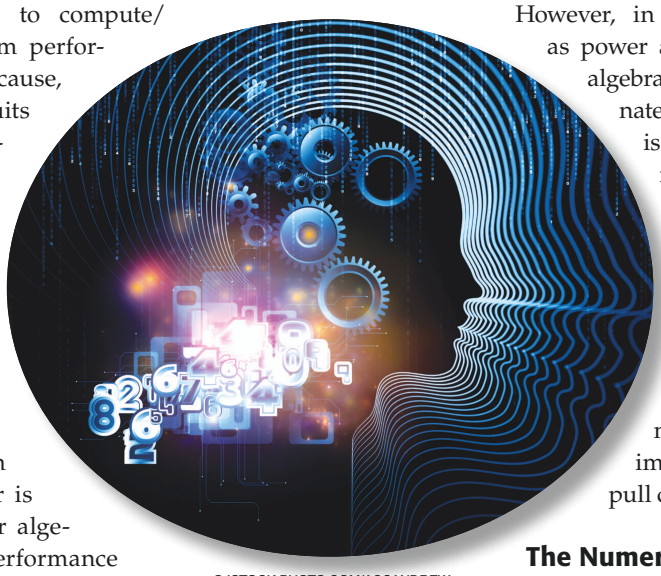

© ISTOCK PHOTO.COM/AGSANDREW

However, in electronic systems such as power amplifiers and oscillators, algebraic design aids, unfortunately, are not available. This is because these applications require operation of the transistor in its nonlinear domain. In these circuits, the performance predictions and circuit design insight are either provided numerically, by CAD simulations using nonlinear models, or experimentally, by measured load-pull contours.

The Numerical Approach to Nonlinear Design

Consider the numerical approach. In this case, the designer of nonlinear circuits usually relies on supplied nonlinear analytical-compact transistor models [3]–[5], which, when properly used within the simulator, should allow for designs to meet the system

M. Fernández-Barciela (monica.barciela@uvigo.es) is with the Signal Theory and Communications Department, Universidad de Vigo, Vigo 36310, Spain. A.M. Pelaez-Perez (anapel@televes.com) is with TELEVES S.A., Santiago 15706, Spain. S. Woodington (simonwoodington@mesuro.com) is with MESURO Ltd, Pencoed CF35 5HZ, United Kingdom. J.I. Alonso (ignacio@gmr.ssr.upm.es) is with the Signals, Systems, and Radiocommunications Department, Universidad Politécnica de Madrid, Madrid 28040, Spain. P.J. Tasker (Tasker@cardiff.ac.uk) is with the School of Engineering, Cardiff University, Cardiff CF24 3AA, United Kingdom.

Digital Object Identifier 10.1109/MMM.2014.2332851
Date of publication: 8 September 2014

specifications. In this approach, the designers' past experiences and intuition are often critical. For example, the initial use of sound design rules, knowledge about the active device, and mastery of the simulator tools are the keys to success. As the system specifications become more demanding, the required circuit architecture will become more complex. This places higher demands on the functionality and accuracy requirements of the nonlinear analytical-compact transistor models and increases the need for algebraic computations to guide the design flow.

A good example of this is the continuing development of communications systems. Each new generation increases the demands on the high-frequency transceivers. To cope, within the available bandwidth allocations, with the exponential increase in the number of users and transmitted information, engineers have devised complex modulation schemes. These modulation schemes, when coupled with the requirements of "greener" systems, push the design of the nonlinear circuits for the microwave front end to the limit, especially the power amplifier. The designer is then required to target state-of-the-art specifications in terms of bandwidth, power, linearity, and energy-conversion efficiency.

The Experimental Approach to Nonlinear Design

It is quite a challenge to ensure that the nonlinear analytical-compact transistor models can meet the functionality and accuracy requirements that such a complex system design demands. The model extraction/design cycles are more demanding in terms of measurement requirements and can become more time consuming. However, the designer can easily be dealing with a new transistor technology, where a nonlinear model is not available, or an established technology, where the available nonlinear models have been developed for different applications and are not accurate enough for the emerging circuit concepts.

An alternative design approach, often the one of choice for power amplifier designers, is to use experimental information directly for design. The measurement and use of load-pull contours is a classic example [6]. In this case, measurements are performed to experimentally document the nonlinear behavior/performance of the transistor when it is driven into different load impedances. The power performance is displayed in the form of load-pull contours. These, along with gain contours or efficiency contours, can be used to identify the required circuit design specifications and likely system performance. Linear CAD-based circuit synthesis can then be used to facilitate the circuit design. In this case, design success is strongly coupled to the quality and complexity of the experimental tools used or available: vector versus scalar measurements and complexity, i.e., CW or pulsed, fundamental only, or fundamental and harmonics, and so on. Again, the designers' past experience and intuition when specifying these measurements is essential since there are no algebraic tools to guide the process.

In a similar way to *S*-parameters, *X*-parameters can be transformed into the equivalent *Z*-parameters and *Y*-parameters.

Characterization Tools

Clearly, both design approaches have been assisted by the continued development of nonlinear characterization systems [7]. The extraction and functional complexity of nonlinear compact models have been improved via the use of large-signal microwave measurement systems. These systems are capable of measuring and engineering the device under test (DUT) large-signal radio-frequency (RF) voltage and current waveforms [8], [9]. Besides, they also provide the designer with much more application-specific experimental data for use in nonlinear circuit synthesis [10], particularly when targeting, e.g., high-efficiency modes of operation, such as Class B or Class F [11]–[14].

The Analytical Approach to Nonlinear Design

To complement this rapid development of nonlinear measurement tools, the development of an algebraic approach for computing/predicting circuit and system performance to intelligently guide the design flow would be very helpful. With regard to this requirement, it is important to note that these advanced measurement systems have stimulated the development of a new class of behavioral models defined in the frequency domain. Because this new approach is based on a natural extension of the linear parameters formulations into the nonlinear domain, it opens up the possibility of developing a complementary set of algebraic design tools.

Frequency-Domain-Based Behavioral Models

The origin of these behavioral model formulations can be found in the fundamental work of Verspeckt [15] and of Verbeyst and Bossche [16] as well as in its transformation into the polyharmonic distortion (PHD) model [17], [18]. This has triggered a number of frequency-domain measurement-based behavioral model formulations and parameter definitions: the *X*-parameters [19] [20], *S*-functions [21], and the Cardiff model [22], [23]. For a more in-depth discussion on the topic of frequency-domain-based behavioral models, the reader is referred to *IEEE Microwave Magazine* review articles [10], [18], and [24]. Most of these proposals diverge on the approach taken to model the complexity required to describe the device nonlinear behavior over a large parameter space, i.e.,

The designer can easily be dealing with a new transistor technology, where a nonlinear model is not available.

fundamental load-pull behavior over the full Smith chart. These models have been successfully used in device nonlinear characterization and in design and modeling of different microwave nonlinear circuits [25]–[29]. Their advantages and drawbacks have been extensively highlighted [8], [24], and tools for their extraction and use in simulators have been developed [30], [31].

Now consider the application of these models to describe the key nonlinear design characteristic, i.e., fundamental load-pull. In the linear-design domain, the electronic two-port system is mathematically described using the following generic linear expression:

$$U_p = F_{p1}(V_1^{\mathrm{DC}}, V_2^{\mathrm{DC}}).W_1 + F_{p2}(V_1^{\mathrm{DC}}, V_2^{\mathrm{DC}}) \cdot W_2. \quad (1)$$

U_p quantifies the generic linear response of the system at port p to the generic stimulus $W_1(\omega)$ at the input port and the generic stimulus $W_2(\omega)$ at the output (load) port. These quantities, U_p and W_p, are usually described as "complex phasors" and could be traveling voltage, current, or power waves. The system is then modeled by the "behavior" complex parameters F_{pn} ("black box" approach), defined at a given static operating point. For example, if U_p is the scattered "b" traveling-voltage wave at port p (1 or 2), and W_1 and W_2 are the incident "a" traveling-voltage waves at port 1 and 2, respectively, then the parameters F_{pn} are the "S-parameters" of the system. From such parameters, algebraically defined design aids, such as gain circles and stability circles, can be computed. In addition, performance figures of merit, such as the maximum available power gain, and design targets, such as optimum input and output match for maximum transducer power gain, can be determined.

Can the frequency-domain-based nonlinear modeling perform the same function? The authors of these behavioral model formulations identified that a nonlinear system (time invariant), over a limited but design relevant stimulus W_2 perturbation space about a reference value W_2^{ref} can, in fact, be accurately mathematically described, in the large-signal steady state. Consider using the following generic expression:

$$U_{p,1} = F_{p1}(\mathrm{LSOP}) \cdot W_1 + F_{p2}(\mathrm{LSOP}) \cdot W_2 + G_{p2}(\mathrm{LSOP}) \cdot W_2^*. \quad (2)$$

Equation (2) represents an extension of (1) that enables improved modeling of a system response into the nonlinear domain. $U_{p,1}$ represents the nonlinear response of the system at port p at the fundamental frequency. F_{p1}, F_{p2}, and G_{p2} are complex parameters defined for a given large-signal operating point (LSOP). The significance of W_2^* is explained in [18]. The LSOP may be described in terms of the static operating point, the magnitude of the input stimuli $|W_1|$, and the reference value of output stimulus W_2^{ref}. A key feature in this formulation is that the behavioral parameter values are independent on W_2. Since the stimulus reference W_2^{ref} can be related to a fixed fundamental reference impedance, the behavioral model parameters can be considered to be mathematically load-independent. This formulation becomes sufficiently simplified to allow analytical design calculations. Hence, it enables the development of a similar set of algebraically defined design aids, as in the case of S-parameters, but also valid in the large-signal regime. The only caution in this approach is to consider the range of validity of (2) when considering the load-independence of the behavioral model parameters. Studies of this range and how to improve the accuracy of these parameters for a given design application have been done experimentally in [32]. However, an important conclusion is that this region is very difficult to predict and model. To improve the model accuracy, we may use a higher-order behavioral model in the generation/extraction at the desired target LSOP for our application [17], [23]. A search procedure during measurements can also be used to find the appropriated LSOP [32]. The optimum/appropriate large-signal load impedance, in this case, is defined as Z_{ref}. A summary of this last approach can be found in "Search Algorithm for Accurate Behavioral Model Parameter Extraction."

Parameter Transformation

Consider the formulation of (2) in the traveling-voltage-wave domain using, for example, the X-parameter terminology of Agilent and assuming phase stimulus A_{11} as zero. (An introduction to X-parameters can be found in [20].) Alternatively, this could also be done in terms of S-functions or coefficients of the Cardiff model:

$$B_{p,1} = \left(\frac{X^F}{A_{11}}\right) \cdot A_{11} + X^S \cdot A_{21} + X^T \cdot A_{21}^*. \quad (3)$$

In a similar way to S-parameters, these traveling-wave behavioral model parameters, i.e., X-parameters, can be transformed into the equivalent Z-parameters, (4), and Y-parameters, (5), considering the algebraic transformations given in "Parameter Transformations."

$$V_{p,1} = \left(\frac{Z^F}{I_{11}}\right) \cdot I_{11} + Z^S \cdot I_{21} + Z^T \cdot I_{21}^* \quad (4)$$

$$I_{p,1} = \left(\frac{Y^F}{V_{11}}\right) \cdot V_{11} + Y^S \cdot V_{21} + Y^T \cdot V_{21}^*. \quad (5)$$

Note that the terms Z^F and Y^F actually refer to voltage or current sources, respectively, and not impedances or admittances as do the rest of the parameters.

At port 2, considering only the fundamental terms, (4) can be written as

Search Algorithm for Accurate Behavioral Model Parameter Extraction

The generic behavioral model formulation given in (3) is capable of being used to provide closed-form expressions to aid in linear and nonlinear circuit designs. However, because of the limited number of terms involved in its formulation, it is only accurate in the vicinity of the LSOP about which they are measured. In this case, this formulation simplicity results in limiting their accuracy in large-signal operation to an area around the fixed load impedance, reference impedance Z_{ref}, set during behavioral model parameter measurement. The higher the power level is, the more compromised the model accuracy. Figure S1 shows the accuracy, in terms of (S1), of a 50-Ω *X*-parameter model with respect to measurements of a heterojunction bipolar transistor (HBT) at two power levels (small signal and 1-dB compression point). As can be seen for small input power levels linear operation, the area of good prediction is the complete Smith chart, but, at higher power levels, the area of good prediction is reduced. Its shape is far from regular and gets distorted and compressed. Hence, when using these behavioral model parameters to predict circuit performance, the selection of the reference impedance Z_{ref} is important to ensure accurate design predictions. This can be achieved using a combined measurement-model extraction procedure, based on an analytic-blind-search interactive process [32] and summarized in Figure S2. The measurement system used in this process for behavioral model parameter measurement was a nonlinear vector network analyzer (NVNA) with a passive tuner at the output port (load) used to adjust/set the reference impedance Z_{ref}:

$$\text{Error}\,(\%) = \left| \frac{P_{out}^{PHD}\,(\text{watts}) - P_{out}^{meas}\,(\text{watts})}{P_{out}^{meas}\,(\text{watts})} \right| \cdot 100\%. \quad \text{(S1)}$$

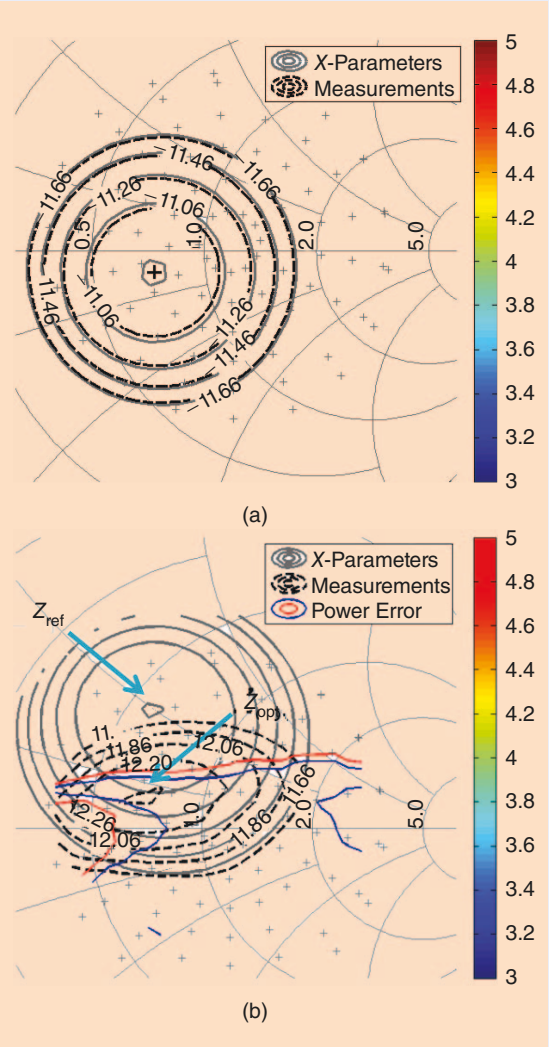

Figure S1. *The HBT PHD 50-Ω model (solid) and load-pull measured (dotted) output power contours. The step size between every two power contours is 0.2 dB. The load-pull grid for the measurements is plotted with gray marks. The input drive is set to (a) −20-dBm and (b) 1-dB compression points. The error contour level percentages, computed through (S1), are indicated in the color bar.*

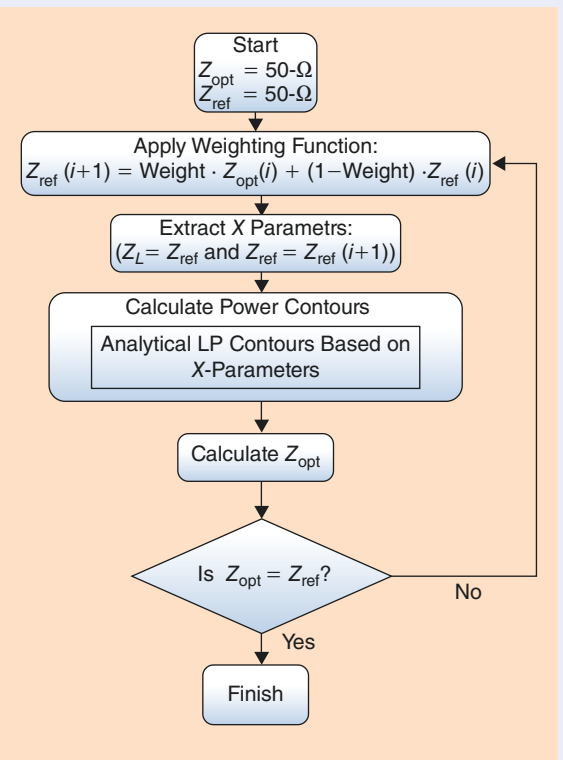

Figure S2. *The blind iterative procedure to extract a behavioral model accurate at a design-oriented terminal impedance.*

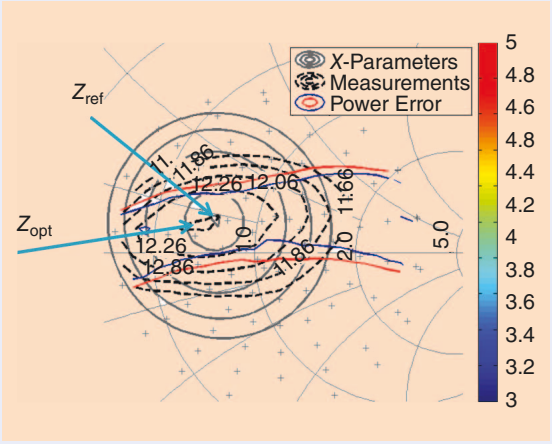

Figure S3. *The HBT PHD model extracted at $Z_{ref} = Z_{opt} = 37 + 7j\ \Omega$ (solid) and the load-pull measured (dotted) output power contours. The step size between every two power contours is 0.2 dB. The error contour levels are indicated in the color bar. The load-pull grid for the measurements is plotted with gray marks. The input drive is set to 1-dB compression point.*

The first step in this process is to determine the initial reference impedance to be used to when extracting the first DUT behavioral model parameters, i.e., *X*-parameters. If we assume that there is no previous knowledge of the active device nonlinear behavior, then the starting impedance ($Z_{ref}(i = 1)$) might be set to 50-Ω.

If the impedance location (Z_{opt}) to achieve the design goal (i.e., maximize output power) computed from these initial behavioral model parameters is close to 50 Ω, the current reference impedance ($Z_{ref}(i = 1)$), we can be confident in the predicted design outcome and continue with the design process. If not, measurements need to be refocused around a new reference impedance ($Z_{ref}(i = 2)$). This new location can be identified by using *X*-parameter analytical computations based on the present behavioral model parameters. For, say, a design target of maximum output power, analytical constant power contour calculation would be used.

To ensure numerical stability (convergence) in practice, it is more appropriate to use a weighted average of (Z_{opt} and $Z_{ref}(i)$) to define the new impedance location:

$$Z_{ref}(i+1) = \text{weight} \cdot Z_{opt}(i) + (1 - \text{weight}) \cdot Z_{ref}(i). \tag{S2}$$

Once the new impedance location is determined and set using the passive tuner, a new set of behavioral model parameters, i.e., *X*-parameters, can be measured. This process will be repeated until convergence between the design impedance space required (Z_{opt}) and the measurement impedance space required $Z_{ref}(i + 1)$, computed using the present set of behavioral model parameters measured at $Z_{ref}(i)$, is achieved. Figure S3 shows the outcome of this procedure on the studied example for the 1-dB compression point. At convergence, power-performance predictions using the behavioral model parameters are capable of providing an accurate design aid.

$$V_{2,1} = Z_{21}^{F} + Z_{22}^{S} \cdot I_{21} + Z_{22}^{T} \cdot I_{21}^{*}. \tag{6}$$

Thus, the corresponding *Z*-parameters, as functions of the *X*-parameters, are those shown in Table 1.

Similarly, at port 2, (5) can be written as

$$I_{2,1} = Y_{21}^{F} + Y_{22}^{S} \cdot V_{21} + Y_{22}^{T} \cdot V_{21}^{*}. \tag{7}$$

Thus, the corresponding *Y*-parameters, as functions of the *X*-parameters, are those shown in Table 1.

In circuit analysis, *Z*-parameters can be used to analyze series connections of two-port networks, while *Y*-parameters can be used to analyze parallel connections of two-port networks. Clearly, from a combination of these two operations, any circuit topology can be analyzed using the transformed nonlinear behavioral model parameters.

Next, we will consider the use of these behavioral nonlinear parameters in the analytical analysis of a simple nonlinear circuit. The example selected in this article is the analysis of the impact of a series feedback, which has relevance in both power amplifier and oscillator design.

Analytical Analysis of Series Feedback

In the design of broadband amplifiers and oscillators, it is quite common to add series feedback to the active device. Typically, it is not practical to fabricate the required RF test structures, to enable direct experimental measurement of the nonlinear behavior of the active device with series feedback. However, if this device nonlinear behavior is measured and described by the behavioral model parameters given by (3), these device behavioral model parameters can be analytically transformed. This is an analytical computation operation that is very fast to perform; hence, the result is instantaneously available, displayed in real time. Through (6), the behavioral model parameters for the device including a series feedback connection of a known *Z*-parameters network (Figure 1) can be computed [33].

Applying (6) [or (S10) in "Parameter Transformations"], the nonlinear series configuration can be computed by the summation of each voltage vector [*V*]. For the particular case in which one of the networks is passive, which is very common in microwave subsystems,

TABLE 1. Parameter transformation.

***X* to *Z* Transformation**		***X* to *Y* Transformation**	
$Z_{21}^{F} = \frac{L_F \cdot K_S^* + L_F^* \cdot K_T - K_F \cdot K_S^* - K_F^* \cdot K_T}{\lvert K_S \rvert^2 - \lvert K_T \rvert^2}$	(8)	$Y_{21}^{F} = \frac{K_F \cdot L_S^* + K_F^* \cdot L_T - L_F \cdot L_S^* - L_F^* \cdot L_T}{\lvert L_S \rvert^2 - \lvert L_T \rvert^2}$	(11)
$Z_{22}^{S} = \frac{L_S \cdot K_S^* - L_T^* \cdot K_T}{\lvert K_S \rvert^2 - \lvert K_T \rvert^2}$	(9)	$Y_{22}^{S} = \frac{K_S \cdot L_S^* - K_T^* \cdot L_T}{\lvert L_S \rvert^2 - \lvert L_T \rvert^2}$	(12)
$Z_{22}^{T} = \frac{L_S^* \cdot K_T - L_T \cdot K_S^*}{\lvert K_S \rvert^2 - \lvert K_T \rvert^2}$	(10)	$Y_{22}^{T} = \frac{K_S^* \cdot L_T - K_T \cdot L_S^*}{\lvert L_S \rvert^2 - \lvert L_T \rvert^2}$	(13)
Auxiliary Parameters		**Auxiliary Parameters**	
$K_F = \frac{X_{21}^{F*} \cdot X_{21,21}^{T} - X_{21}^{F} \cdot (1 + X_{21,21}^{S*})}{\lvert 1 + X_{21,21}^{S} \rvert^2 - \lvert X_{21,21}^{T} \rvert^2}$	(14)	$L_F = \frac{X_{21}^{F*} \cdot X_{21,21}^{T} + X_{21}^{F} \cdot (1 - X_{21,21}^{S*})}{\lvert 1 - X_{21,21}^{S} \rvert^2 - \lvert X_{21,21}^{T} \rvert^2}$	(17)
$K_S = \frac{(1 + X_{21,21}^{S*})}{\lvert 1 + X_{21,21}^{S} \rvert^2 - \lvert X_{21,21}^{T} \rvert^2}$	(15)	$L_S = \frac{Z_c \cdot (1 - X_{21,21}^{S*})}{\lvert 1 - X_{21,21}^{S} \rvert^2 - \lvert X_{21,21}^{T} \rvert^2}$	(18)
$K_T = \frac{X_{21,21}^{T}}{\lvert 1 + X_{21,21}^{S} \rvert^2 - \lvert X_{21,21}^{T} \rvert^2}$	(16)	$L_T = \frac{-Z_c \cdot X_{21,21}^{T}}{\lvert 1 - X_{21,21}^{S} \rvert^2 - \lvert X_{21,21}^{T} \rvert^2}$	(19)

the incorporation of a series configuration (Figure 1) can be analytically described by

$$[V] = [X^F]^a + ([X^{ST}]^a + [\mathrm{Id}]) \cdot ([\mathrm{Id}] - [X^{ST}]^a)^{-1} \cdot ([X^F]^a + Z_c[I]) + [Z^b] \cdot [I], \quad (20)$$

where $[Z^b]$ is the Z-parameters of the passive network (provided this network can be characterized in terms of those parameters), Z_c is the characteristic impedance (a real number), $[I]$ is a column vector formed by $I_{p,1}$ current terms and their conjugates, $[V]$ is a column vector composed of $V_{p,1}$ voltage terms and their conjugates, and $[\mathrm{Id}]$ is the identity matrix.

This computed current–voltage relationship can now be transformed back into traveling-voltage-wave domain through (S12) and (S13) in "Parameter Transformations," thus obtaining

$$[B] = \frac{1}{2} \times \begin{pmatrix} (([X^{ST}]^a + [\mathrm{Id}]) \cdot ([\mathrm{Id}] - [X^{ST}]^a)^{-1} \cdot Z_c + [Z^b] - Z_c \cdot [\mathrm{Id}]) \cdot \\ (([X^{ST}]^a + [\mathrm{Id}]) \cdot ([\mathrm{Id}] - [X^{ST}]^a)^{-1} \cdot Z_c + [Z^b] + Z_c \cdot [\mathrm{Id}])^{-1} \cdot \\ (2[A] - [X^F]^a - ([X^{ST}]^a + [\mathrm{Id}]) \cdot ([\mathrm{Id}] - [X^{ST}]^a)^{-1} \cdot [X^F]^a) \\ + [X^F]^a + [X^F]^a \cdot ([X^{ST}]^a + [\mathrm{Id}]) \cdot ([\mathrm{Id}] - [X^{ST}]^a)^{-1} \end{pmatrix}. \quad (21)$$

Hence, in summary, the behavioral model parameters, X-parameters, of the device with a known series connection can be computed from the measured device behavioral model parameters, X-parameters, using the following:

$$[X^F] = \frac{1}{2} \times \begin{pmatrix} (([X^{ST}]^a + [\mathrm{Id}]) \cdot ([\mathrm{Id}] - [X^{ST}]^a)^{-1} \cdot Z_c + [Z^b] - Z_c \cdot [\mathrm{Id}]) \cdot \\ (([X^{ST}]^a + [\mathrm{Id}]) \cdot ([\mathrm{Id}] - [X^{ST}]^a)^{-1} \cdot Z_c + [Z^b] + Z_c \cdot [\mathrm{Id}])^{-1} \cdot \\ (-[X^F]^a - ([X^{ST}]^a + [\mathrm{Id}]) \cdot ([\mathrm{Id}] - [X^{ST}]^a)^{-1} \cdot [X^F]^a) \\ + [X^F]^a + [X^F]^a \cdot ([X^{ST}]^a + [\mathrm{Id}]) \cdot ([\mathrm{Id}] - [X^{ST}]^a)^{-1} \end{pmatrix}. \quad (22)$$

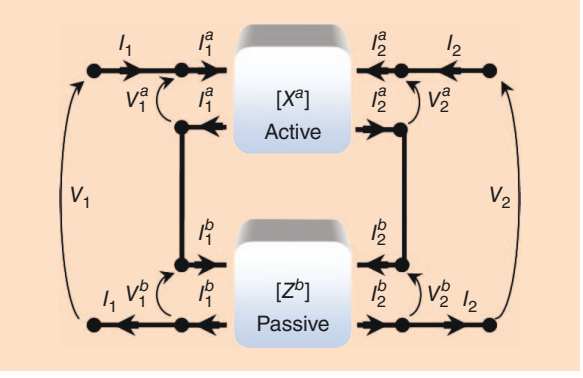

Figure 1. *The series connection of two-port networks. (Figure adapted from [33].)*

$$[X^{ST}] = (([X^{ST}]^a + [\mathrm{Id}]) \cdot ([\mathrm{Id}] - [X^{ST}]^a)^{-1} \cdot Z_c + [Z^b] - Z_c \cdot [\mathrm{Id}]) \cdot (([X^{ST}]^a + [\mathrm{Id}]) \cdot ([\mathrm{Id}] - [X^{ST}]^a)^{-1} \cdot Z_c + [Z^b] + Z_c \cdot [\mathrm{Id}])^{-1}, \quad (23)$$

where $[\mathrm{Id}]$ is the identity matrix. Note that there is a special case when the port impedances are equal to the negative of Z_c, in which case the $V/I\,(Z)$ to $A/B\,(X)$ parameter conversions cannot be performed [34].

The new combined behavioral model parameters, X-parameters, still have a design-relevant load impedance area where they remain valid for modeling purposes. Note that, when the feedback is added to the active device, a translation of this load space is produced. At the device plane, this is still the optimum location since the output impedance seen by the transistor remains unchanged. Figures 2 and 3 show an example of validation of these expressions at 5 GHz. In this case, an RF-test structure consisting of a silicon–germanium (SiGe) HBT with series capacitive feedback is shown in Figure 3(a); it is constructed and its nonlinear behavior is directly characterized using an NVNA. Figures 2 and 3(b) compare the test structure

Parameter Transformations

If we consider the simplified behavioral model parameter formulation in (2), considering only the fundamental and second harmonics terms, the system response at port 2 in matrix format can be described as follows:

$$\begin{bmatrix} B_{2,1} \\ B^*_{2,1} \\ B_{2,2} \\ B^*_{2,2} \end{bmatrix} = \begin{bmatrix} X^F_{21} \\ X^{F*}_{21} \\ X^F_{22} \\ X^{F*}_{22} \end{bmatrix} + \begin{bmatrix} X^S_{21,21} & X^T_{21,21} & X^S_{21,22} & X^T_{21,22} \\ X^{T*}_{21,21} & X^{S*}_{21,21} & X^{T*}_{21,22} & X^{S*}_{21,22} \\ X^S_{22,21} & X^T_{22,21} & X^S_{22,22} & X^T_{22,22} \\ X^{T*}_{22,21} & X^{S*}_{22,21} & X^{T*}_{22,22} & X^{S*}_{22,22} \end{bmatrix} \cdot \begin{bmatrix} A_{21} \\ A^*_{21} \\ A_{22} \\ A^*_{22} \end{bmatrix}. \tag{S3}$$

In the complex phasors $B_{p,m}$, A_{qn} and complex parameters X^F_{pm}, $X^S_{pm,qn}$, and $X^T_{pm,qn}$, $p(2)$ and $q(1,2)$ are the port indexes, $m(1,2)$ and $n(1,2)$ are the harmonic indexes. A matrix description of (S3) would be

$$[B(\mathrm{DC}, |A_{11}|)] = [X^F(\mathrm{DC}, |A_{11}|)] + [X^{ST}(\mathrm{DC}, |A_{11}|)] \cdot [A(\mathrm{DC}, |A_{11}|)]. \tag{S4}$$

We can transform (S4), to obtain the Z-parameters matrix, considering the relationship between voltage or current, and incident and scattered traveling waves. In matrix format, this relationship can be expressed as

$$[V] = [A] + [B] \tag{S5}$$

$$[I] = \frac{([A] - [B])}{Z_c}. \tag{S6}$$

Using (S4) in (S5), and rearranging terms, we obtain

$$[V] = [X^F] + ([X^{ST}] + [Id])[A]. \tag{S7}$$

Then,

$$[A] = ([X^{ST}] + [Id])^{-1} \cdot ([V] - [X^F]). \tag{S8}$$

Similarly, using (S4) in (S6) and rearranging terms we obtain

$$[A] = ([\mathrm{Id}] - [X^{ST}])^{-1} \cdot ([X^F] + Z_c[I]). \tag{S9}$$

Therefore, making both expressions equal for the A-waves, (S8) and (S9), we obtain the relationship between the voltage and current vectors

$$[V] = [X^F] + ([X^{ST}] + [\mathrm{Id}]) \cdot ([\mathrm{Id}] - [X^{ST}])^{-1} \cdot ([X^F] + Z_c \cdot [I]), \tag{S10}$$

where Z_c is the characteristic impedance, a real number; $[I]$ is a column vector of $I_{p,m}$ current terms and their conjugates; and, finally, $[V]$ is a column vector of $V_{p,m}$ voltage terms and their conjugates. Note that the inverse matrix exists if its determinant is not zero; for physically valid X-parameter values, the inverse matrix must exist.

Equation (S10) can be used to obtain Z-parameters as functions of the X-parameters. Similarly, we can obtain the matrix expression of the terminal currents as functions of the terminal voltages and the X-parameters:

$$[I] = -1/Z_c \cdot [X^F] + 1/Z_c \cdot (([\mathrm{Id}] - [X^{ST}]) \cdot ([X^{ST}] + [\mathrm{Id}])^{-1} \cdot (-[X^F] + [V]). \tag{S11}$$

From this expression, we would identify the Y-parameters as functions of the X-parameters. This formulation may also be used to compute series and parallel network connections.

In the case of transforming Z-parameters back to X-parameters, it is helpful to make use of the following relationships:

$$[A] = \frac{([V] + Z_c[I])}{2} \tag{S12}$$

$$[B] = \frac{([V] - Z_c[I])}{2}. \tag{S13}$$

measured performance to that predicted from the device measurements without a feedback component, at different output power levels and output impedances.

These results are proof that we can use this behavioral formulation to predict not only cascaded network connections but also series network connections analytically. While we have not provided experimental proof, we hope the reader will accept that we can use the Y-parameters in a similar way to predict parallel network connections.

Analytical Determination of Load-Pull Contours and Optimum Impedance

Other design aids that may be useful to designers of nonlinear circuits are analytic expressions to provide early predictions of the large-signal power contours and the optimum impedance for maximum output power. Usually, load-pull contours are only obtained after performing measurements or simulations with a compact model or a load-dependent behavioral model [35], [23] over a large set of load impedances. In all these cases, this can be time-consuming. Analytic calculations of these curves from a reduced set of behavioral model parameters, determined after a limited number of measurements or simulations at a selected or initial Z_{ref} can speed up the load-pull measurement [36] or design procedures [37].

To enable this functionality, closed-form expressions for the power contours and the optimum impedance as function of the device behavioral model parameters have been derived [32]. Figure 4 shows a general schematic diagram of a transistor with input and output

matching networks. In this figure, the different parameters we will use in the development of the algebraic expressions are defined.

We can express the RF power P_{out} delivered at the transistor output at the fundamental frequency in terms of traveling-voltage waves at that transistor port as

$$P_{out} = \frac{1}{2Z_C}(|B_2|^2 - |A_2|^2). \quad (24)$$

Using (3), to describe B_2 in terms of A_2 waves through the transistor behavioral model parameters; load-independent X-parameters, we obtain the closed-form (25) that is able to predict the output fundamental power

$$P_{out} = \frac{1}{2Z_C}(|X_{21}^F + X_{22}^S A_2 + X_{22}^T A_2^{*}|^2 - |A_2|^2). \quad (25)$$

The simplified formulation used in (25) assumes that all the harmonic terminations are 50-Ω. As a consequence, the A_{qn} waves (following the index notation in [32]) can be neglected for $n > 1$. The A_{qn} waves only have a fundamental frequency component; the harmonic indexes in (25) are equal to $m = n = 1$. This is why we do not explicitly write these indexes in (25) to simplify notation. This "one harmonic" approximation is valid, for example, in oscillator design, provided the resonator quality factor is large, since the harmonic components will be drastically attenuated. Otherwise, the accuracy in the prediction will decrease, but we will still have better predictions than when using S-parameters. The above assumption will be considered for the rest of the expressions.

These advanced measurement systems have stimulated the development of a new class of behavioral models defined in the frequency domain.

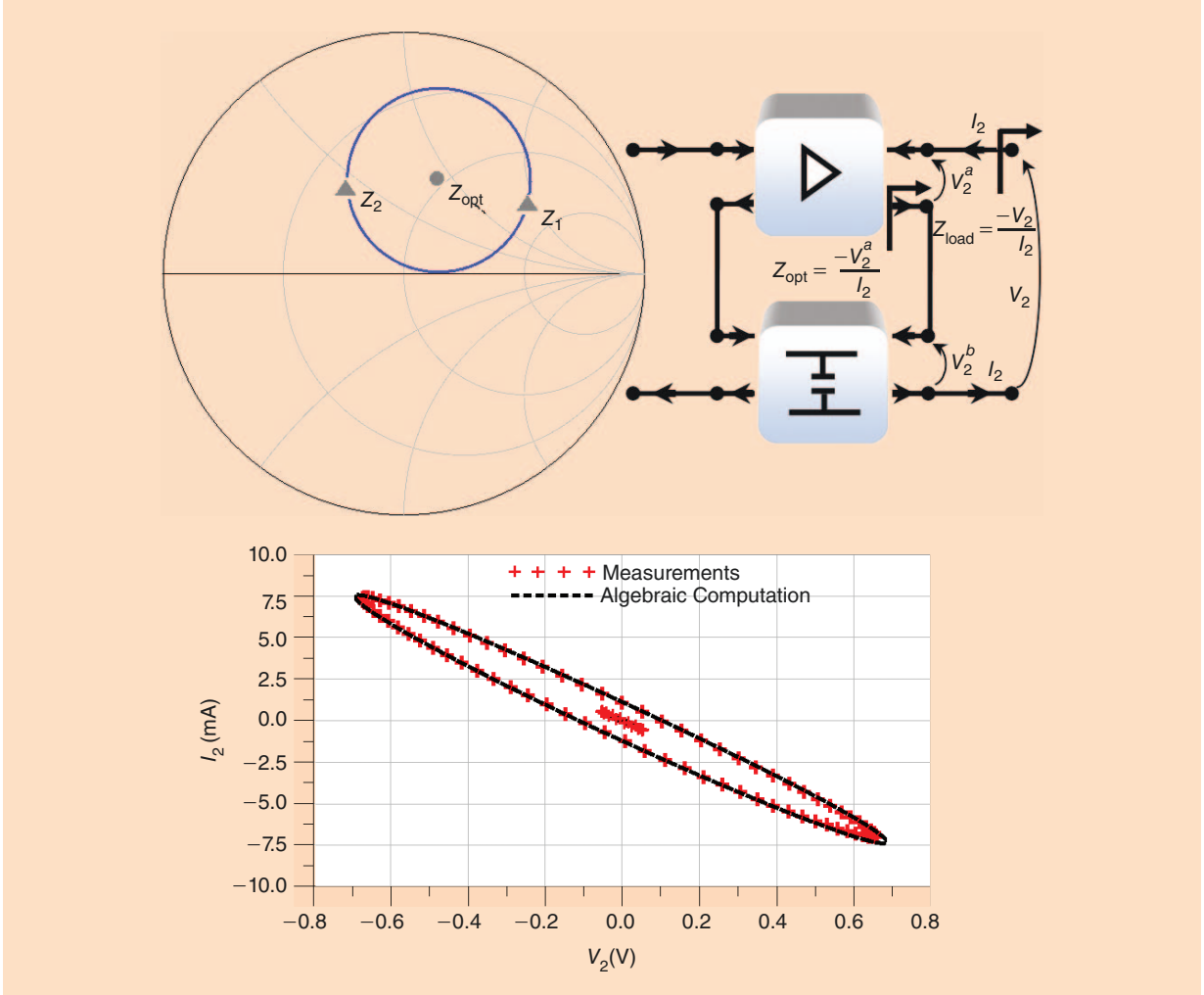

Figure 2. *Large-signal (1-dB compression point) and small-signal (−25-dBm) output RF loadlines at Z_{opt}. The behavioral model was extracted at Z_{opt}, which was determined using the search algorithm described previously. The transistor load impedances investigated to check impedance range validity, in Figure 3, are shown on the Smith chart: $Z_1 = 68 + 19.2j\ \Omega$, $Z_2 = 17 + 4.8j\ \Omega$, and $Z_{opt} = 34 + 9.6j\ \Omega$. (Figure adapted from [33].)*

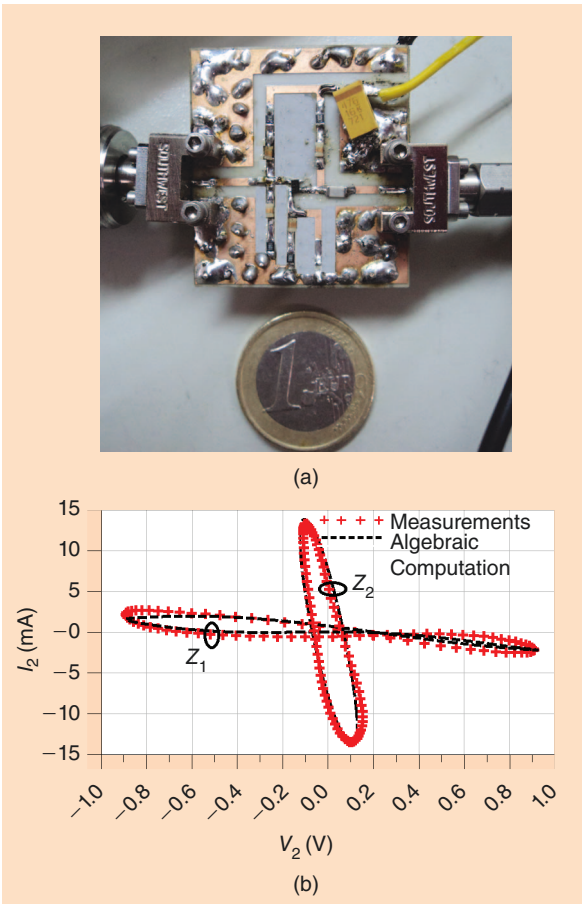

Figure 3. *(a) The manufactured series configuration in hybrid microwave integrated circuit (HMIC) technology. (b) The measured and modeled large-signal RF output behavior at the Z_1 and Z_2 load impedances (Figure 2). Note that, in this case, the behavioral model is extrapolating from the measured performance at Z_{opt}. (Figure adapted from [33].)*

Equation (25) can be expanded and rearranged into an equation that has the form of a general conic section, specifically an ellipse, representing a contour of constant power on A_2, on the condition that

$$|X_{21}^F|^2 - 2Z_C P_{out} \neq 0. \tag{26}$$

The contour of constant power can then be represented by (27), which is the polar form of an ellipse, such as the one represented in Figure 5. The full derivation of (27) can be found in [32] and [37]

$$\begin{aligned} C(\phi) = C_E &+ (r_A \cos(\phi)\cos(\theta) + r_B \sin(\phi)\sin(\theta)) \\ &+ j(r_A \cos(\phi)\sin(\theta) - r_B \sin(\phi)\cos(\theta)), \end{aligned} \tag{27}$$

where ϕ is the phase on the A_2 plane, which is in the range between zero and 2π; θ is the ellipse's main axis angle; C_E is the center; and r_A and r_B are the ellipse radii (Figure 5).

The ellipse parameters are functions of the behavioral model parameters, X-parameters, and can be obtained through the following:

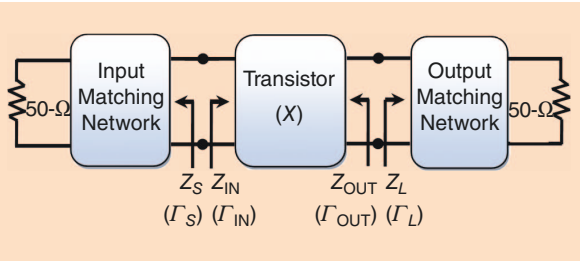

Figure 4. *A schematic shows the definition of the impedances and reflection coefficients used in the analysis.*

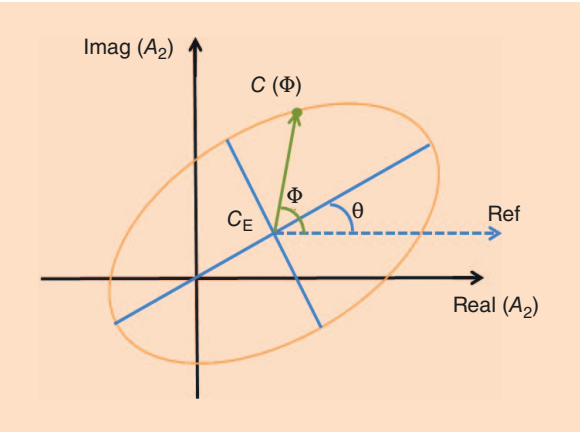

Figure 5. *The definition of the contour of constant power on the A_2 plane.*

$$C_E = -\alpha - j\beta \tag{28}$$

$$\alpha = \frac{D - 2B\beta}{2A} \tag{29}$$

$$\beta = \frac{-(AE - DB)}{2(B^2 - AC)} \tag{30}$$

$$\tan(2\theta) = \frac{2B}{A - C} \tag{31}$$

$$r_A = \sqrt{\left|\frac{-K}{A\cos^2(\theta) + C\sin^2(\theta) + B\sin(2\theta)}\right|} \tag{32}$$

$$r_B = \sqrt{\left|\frac{-K}{C\cos^2(\theta) + A\sin^2(\theta) - B\sin(2\theta)}\right|} \tag{33}$$

$$A = ((|X_{22}^S|^2 + |X_{22}^T|^2 - 1) + 2\Re(X_{22}^S X_{22}^{T*})) \tag{34}$$

$$B = -2\Im(X_{22}^S X_{22}^{T*}) \tag{35}$$

$$C = ((|X_{22}^S|^2 + |X_{22}^T|^2 - 1) - 2\Re(X_{22}^S X_{22}^{T*})) \tag{36}$$

$$D = 2\Re(X_{21}^{F*} X_{22}^S + X_{21}^F X_{22}^{T*}) \tag{37}$$

$$E = -2\Im(X_{21}^{F*} X_{22}^S + X_{21}^F X_{22}^{T*}) \tag{38}$$

$$F = |X_{21}^F|^2 - 2Z_C P_{out} \tag{39}$$

$$K = F - A\alpha^2 - C\beta^2 - 2B\alpha\beta. \tag{40}$$

From the expression of the constant power on the A_2 contour (27), the equation for the reflection coefficients at the transistor output terminals compatible with A_2 can be easily obtained through (41). The results can be seen in Figure 6:

$$\Gamma_L(\phi) = \frac{A_2}{B_2} = \frac{C(\phi)}{X_{21}^F + X_{22}^S C(\phi) + X_{22}^T C(\phi)^*}. \quad (41)$$

The maximum output power is located at the center of the ellipse. Therefore, the load impedance for the maximum power design as a function of input power amplitude is given by

$$\Gamma_L\Big|_{\text{power}}^{\text{Max}} = \frac{-\alpha - j\beta}{X_{21}^F + X_{22}^S(-\alpha - j\beta) + X_{22}^T(-\alpha + j\beta)}. \quad (42)$$

Moreover, the maximum transistor output power can also be computed as a function of the X-parameters and, thus, in terms of the input power amplitude from

$$P_{\text{Max}} = \frac{|X_{21}^F|^2 - A\alpha^2 - C\beta^2 - 2B\alpha\beta}{2Z_C}. \quad (43)$$

If the obtained maximum output power closed-form expression is plotted, it can be observed that this function presents a maximum (Figure 6) that may be used as the optimum operation point for maximum oscillator power in the oscillator design. This optimum point corresponds to a terminating impedance that can be calculated through (42). Figure 6 shows the validation of these equations with Advanced Design System simulations using the X-parameters model of a SiGe HBT.

Analytical Determination of Input and Output Reflection Coefficients and Negative Resistance Boundaries

As another example of analytic aids to nonlinear circuit design, we may consider algebraic expressions for the input and output reflection coefficients of a transistor, hence the calculation of the negative resistance boundaries curves between the energy-delivering and energy-absorbing regions on the Smith chart. Note that these parameters are drive-power level dependent [38]. This graphical design guide information is very useful in directing the design of power amplifiers and oscillators. The negative resistance boundaries $|\Gamma_{\text{IN}}| = 1$ or $|\Gamma_{\text{OUT}}| = 1$ have similarities to the linear stability circles, if only from a design point of view. Even though, at small-signal levels, they overlap the stability circles, they are not sufficient to fully predict transistor in-band and out-of-band stability in the large-signal regime.

We can obtain the algebraic expressions of these design parameters by manipulating traveling-wave relationships, as in the case of the power contours and under the same simplifying assumptions [38].

In the case of the input reflection coefficient, we can write

$$\Gamma_{\text{IN}} = \frac{B_1}{A_1} = \frac{X_{11}^S A_1 + X_{12}^S A_2 + X_{12}^T P^2 A_2^*}{A_1}, \quad (44)$$

where $X_{11}^S = \dfrac{X_{11}^F}{|A_{11}|}$

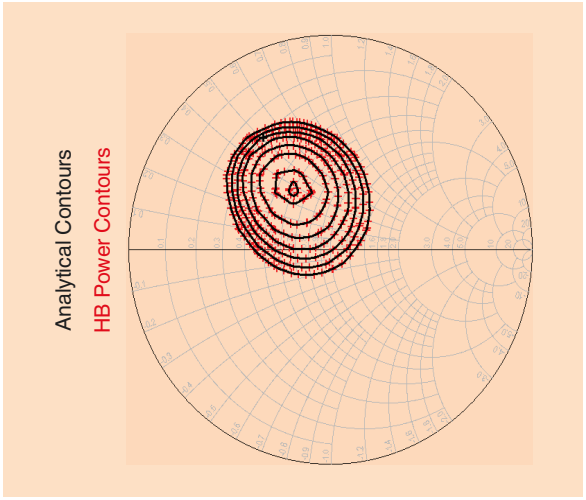

Figure 6. *The 5-GHz HBT load-pull power contours computed by harmonic balance (HB) simulation (plus marks) and analytically, by the algebraic expressions (solid). The step size between power contours is 0.1 dB. The input drive is set to 1-dB compression point.*

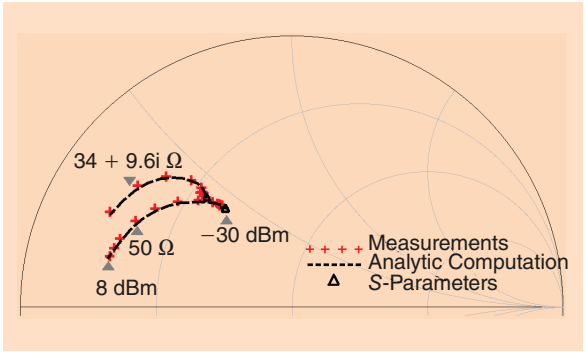

Figure 7. *The HBT measured and modeled (with X-parameters and S-parameters) 5-GHz input reflection coefficient versus input power for two different transistor load impedances: 50 Ω and $Z_{\text{opt}} = 34 + 9.6j$ Ω. Note that the behavioral model used was extracted at $Z_{\text{opt}} = 34 + 9.6j$ Ω, and the harmonic impedances were set to 50 Ω. (Figure adapted from [38].)*

$$\begin{cases} B_2 = \dfrac{A_2}{\Gamma_L} = X_{21}^S A_1 + X_{22}^S A_2 + X_{22}^T P^2 A_2^* \\ B_2^* = \dfrac{A_2^*}{\Gamma_L^*} = X_{21}^{S*} A_1^* + X_{22}^{S*} A_2^* + X_{22}^{T*} P^{-2} A_2. \end{cases} \quad (45)$$

From (45), the A_2 traveling-voltage wave can be expressed as a function of the input wave A_1:

$$A_2 = \frac{((1 - \Gamma_L^* X_{22}^{S*})\Gamma_L X_{21}^S + \Gamma_L X_{22}^T \Gamma_L^* X_{21}^{S*})A_1}{(|\Gamma_L X_{22}^S - 1|^2 - |\Gamma_L X_{22}^T|^2)}. \quad (46)$$

By replacing (46) in (44), we obtain

$$\Gamma_{\text{IN}} = \frac{B_1}{A_1} = X_{11}^S + \frac{X_{12}^S \Gamma_L ((1 - \Gamma_L X_{22}^S)^* X_{21}^S + X_{22}^T \Gamma_L^* X_{21}^{S*})}{(|\Gamma_L X_{22}^S - 1|^2 - |\Gamma_L X_{22}^T|^2)} + \frac{X_{12}^T \Gamma_L^* ((1 - \Gamma_L X_{22}^S) X_{21}^{S*} + X_{22}^{T*} \Gamma_L X_{21}^S)}{(|\Gamma_L X_{22}^S - 1|^2 - |\Gamma_L X_{22}^T|^2)}. \quad (47)$$

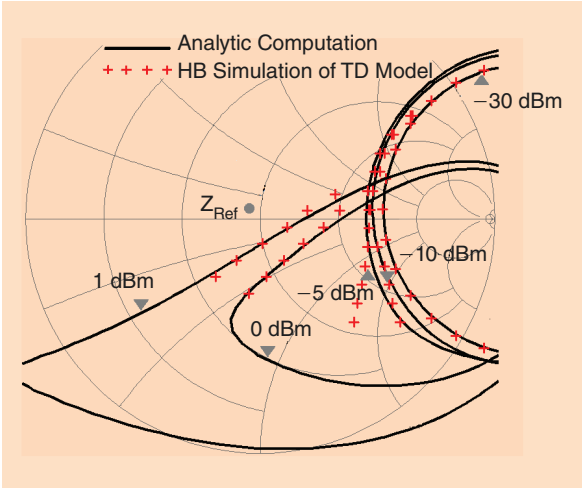

Figure 8. *The large-signal $|\Gamma_{IN}| = 1$ curves of the series connection (Figure 2). The area to the left of the loci corresponds to the negative real-impedance region. The transformed Z_{ref} for the HBT with the series connection is also shown on the plot. (Figure adapted from [38].)*

Figure 7 shows the experimental validation of (47) versus power for an HBT device at two different load impedances. Also shown is the prediction from small signal *S*-parameters, which is clearly drive-level invariant and, hence, erroneous. Even though the *X*-parameters were measured at a load impedance at $Z_{opt} = 34 + 9.6j\Omega$, they are able to provide good predictions with power for a 50-Ω load impedance.

In a similar way, we can obtain the output reflection coefficient as a function of the behavioral model parameters (48)

$$\Gamma_{out} = X_{22}^{S} + X_{21}^{S}\Delta + \frac{X_{22}^{T}\Delta}{\Delta^{*}}, \tag{48}$$

where

$$\frac{A_1}{A_2} = \frac{|\Gamma_S|^2(|X_{12}^{S}|^2 - |X_{12}^{T}|^2)}{(\Gamma_S^{*}X_{12}^{S*}(1-\Gamma_S X_{11}^{S}) - \Gamma_S X_{12}^{T}(1-\Gamma_S^{*}X_{11}^{S*}))} = \Delta. \tag{49}$$

The negative resistance boundary loci between the negative (energy delivered) and positive (energy absorbing) real output/input impedance regions on the corresponding source/load impedance reference plane can be obtained by solving (47) and (48) for $|\Gamma_{IN}| = 1$ and $|\Gamma_{OUT}| = 1$, respectively. The solution $|\Gamma_{IN}| = 1$, loci, located on the load Γ_L plane, lies, in this case, not on a simple circle as in small signal, but on a quartic plane curve that can be expressed by the implicit form in (50). Note that as the input drive is reduced and as the X^T terms tend to zero, this expression simplifies to a simple circle, identical to that predicted by the *S*-parameters and commonly referred to as the "output stability circle."

The solution $|\Gamma_{OUT}| = 1$, loci, located on the source Γ_S plane also lies on a quartic plane curve and its expression is similar to (50) with slightly different terms.

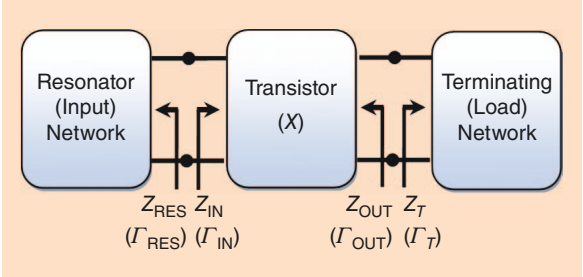

Figure 9. *A schematic of the two-port oscillator, with the definition of the impedances and reflection coefficients used in this section. Note that some of the definitions are different from those used in previous sections.*

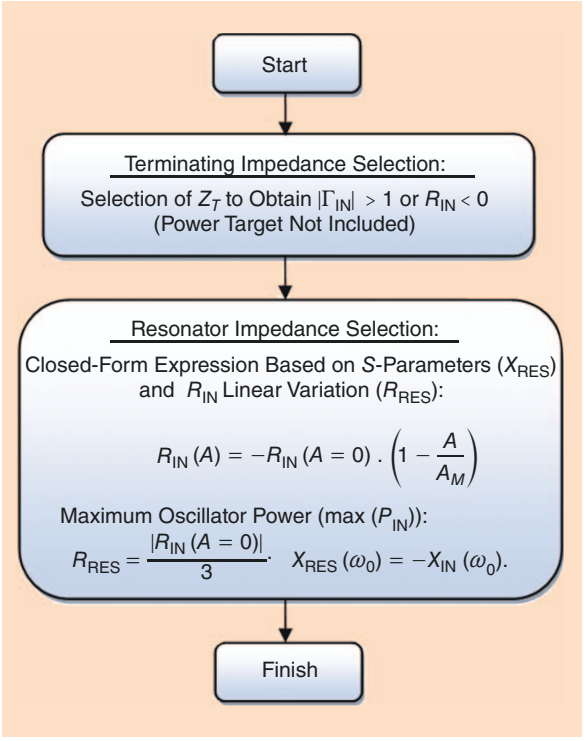

Figure 10. *A flowchart of the negative-resistance method for RF oscillator design.*

$$x^4 + y^4 + 2x^2y^2 + \left(\frac{2\text{real}(d)}{e}\right)x^3 + \left(\frac{-2\text{imag}(d)}{e}\right)y^3 + \left(\frac{2\text{real}(d)}{e}\right)y^2x + \left(\frac{-2\text{imag}(d)}{e}\right)x^2y + \left(\frac{2\text{real}(b)+c}{e}\right)x^2 + \left(\frac{-2\text{real}(b)+c}{e}\right)y^2 + \left(\frac{-4\text{imag}(b)}{e}\right)xy + \left(\frac{2\text{real}(a)}{e}\right)x + \left(\frac{-2\text{imag}(a)}{e}\right)y + \left(\frac{1-|X_{11}^{S}|^2}{e}\right) = 0 \text{ and } \Gamma_L = x + jy, \tag{50}$$

where parameters a, b, c, d, and e can be expressed as a function of the behavioral parameters, as detailed in [38].

Figure 8 shows the validation of (50) at 5 GHz by comparing analytical computations with simulations from a time-domain, table-based model performed on the circuit shown in Figure 2, the HBT with series feedback. The computation of these curves numerically

with HB simulations took approximately 12 min, while the analytical approach allows for instantaneous computation, providing real-time design feedback.

The application of these complex but useful analytical expressions will be considered in the next section.

Case Study: Free-Running Oscillator Design

Free-running oscillators play an important role in the frequency-conversion stages in communication systems [39]. These circuits self-generate a signal whose fundamental frequency strongly depends on the values of the circuit elements. Therefore, the circuit must be accurately designed to obtain the desired oscillation frequency and acceptable performance in terms of RF output power and dc to RF conversion efficiency.

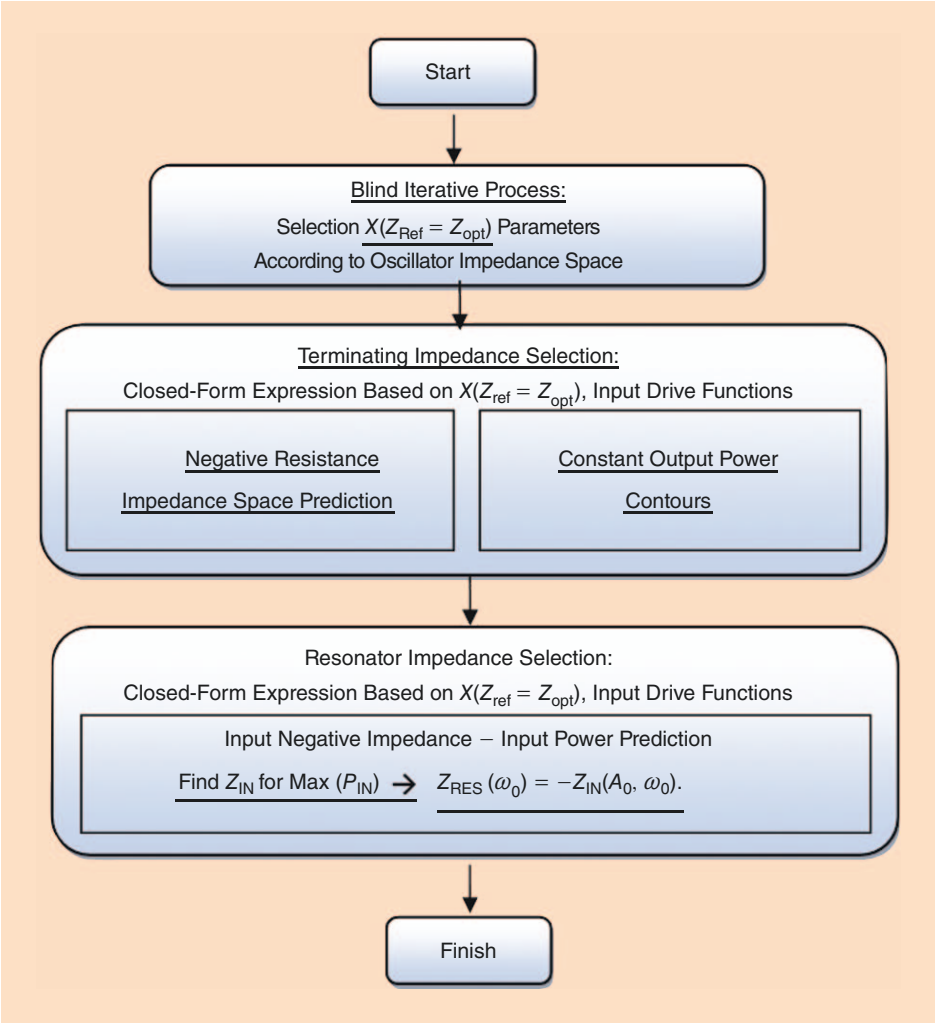

Figure 11. *The nonlinear analytical oscillator design technique.*

Since oscillator design is usually a numerical complex task, aided by nonlinear simulators and nonlinear empirical models (both compact and behavioral [25]), the previously discussed analytical expressions can guide the design flow by providing instantaneous real-time computations of the network nonlinear basic performance.

Our starting point in this case study is the negative-resistance method for RF oscillator design (Figures 9 and 10). This popular analytical procedure is mainly based on a combination of linear assumptions, relying on *S*-parameters coupled with the assumption of a linear dependence of the real input impedance of the active device with the signal amplitude (to compute the resonator resistance for maximum oscillator power) [37]. We will follow this method to design a 5-GHz HBT-based free-running oscillator, but applying the previously developed analytic expressions based on behavioral parameters to account for fundamental nonlinear device behavior.

Note that, in the literature, other methodologies for oscillator design can be found that significantly improve the classic approach shown in Figure 10. This is the case of HB-based numerical design methods,

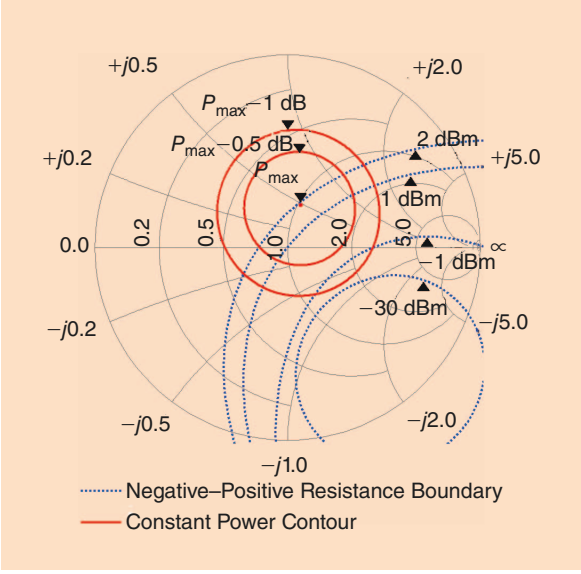

Figure 12. *The input negative resistance boundary and constant power contours of the HBT with series feedback at the fundamental frequency, 5 GHz (load plane). The constant power contours are plotted for* $|A_1| = 0.4$ *(1 dBm).*

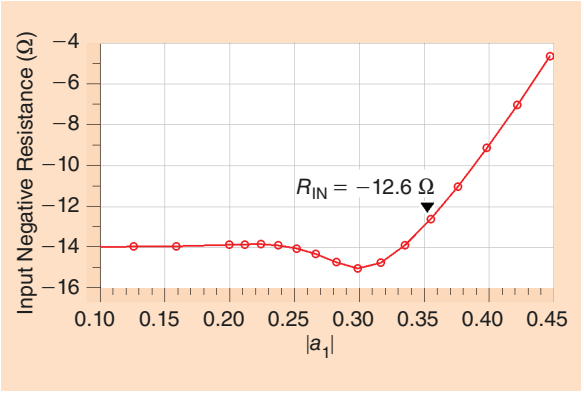

Figure 13. *The input negative-resistance at the network series connection (HBT with feedback and terminating network) computed from (47).*

where the auxiliary generator technique is one of the most extended [40], [41]. Nevertheless, one drawback of this method is the time-consuming, simulator-based oscillator design steps required to obtain an optimum design solution, hence the solution is not always easy to achieve. For this reason, it would still be helpful to guide the numerical procedure using nonlinear analytical design aids, enabling real-time synthesis and quickly providing an initial valid design solution.

The oscillator design procedure considered in this section can be briefly described through the following steps [37], which are summarized in Figure 11.

1) A potentially unstable biased transistor able to provide the desired frequency, output power, and phase noise specifications for the oscillator circuit is selected.
2) The appropriate transistor terminating (output reference) impedance, following the blind iterative process described in "Search Algorithm for Accurate Behavioral Model Parameter Extraction," to obtain, in this example, maximum output power, is selected.
3) The load-independent behavioral transistor model, i.e., *X*-parameters, at the computed (in Step 2) reference output impedance to predict oscillator design impedance space is extracted. Note that Steps 2 and 3 are coupled through the search algorithm.
4) The analytical selection of the terminating load Z_T to simultaneously achieve maximum transistor output power and negative resistance at the transistor input ($|\Gamma_{IN}| > 1$) can now be undertaken.

TABLE 2. The HBT-based oscillator: analytical method versus HB simulation.

	Frequency (GHz)	Power, Fundamental Frequency (dBm)
Analytical *X*-parameters method	5.00	10.61
HB simulation	5.01	10.64

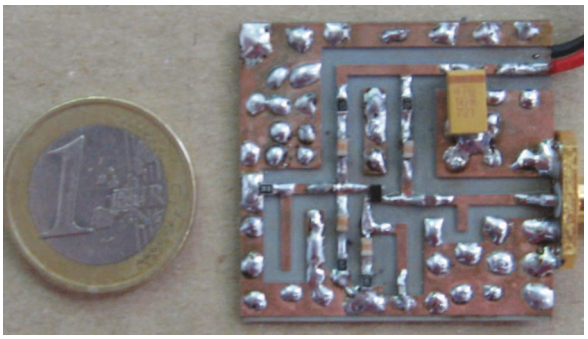

Figure 14. *The common-emitter 5-GHz-based oscillator circuit.*

The determination of the negative resistance space as a function of the input drive is crucial, if we want accurate oscillator design. It is very useful, then, to know $|\Gamma_{IN}| = 1$ boundary versus power at the desired oscillation frequency. For that purpose, we will use the analytical (50) to provide design guidance. Simultaneously, we will use the analytical (41) to predict the output power contours and guide the design toward achieving maximum output power.

Figure 12 shows an example of power contours and $|\Gamma_{IN}| = 1$ curves versus power at 5 GHz for an HBT with capacitive feedback. Behavioral parameters were extracted at $Z_{ref} = 34 + 9.6j\ \Omega$ chosen after following the search algorithm.

5) The resonator (input) impedance Z_{RES} is selected. The nonlinear input impedance (Z_{IN}) may again be computed analytically by means of (47). This power-dependent analytical expression predicts Γ_{IN} of the nonlinear circuit in large-signal operation and from it, the resonator impedance Z_{RES} adequate to obtain maximum steady-state oscillator power.

Figure 13 shows the input resistance, R_{IN}, for the example in Figure 12, which is clearly nonlinear with the input injection. Thus, the linear assumption in the conventional method might produce inaccurate results.

From (47), the power delivered to the resonator by the transistor can be easily determined through

$$P_{RES} = \frac{1}{2Z_C}(|B_1|^2 - |A_1|^2) = \frac{1}{2Z_C}|A_1|^2(|\Gamma_{IN}|^2 - 1). \quad (51)$$

This power, calculated by means of (51), is a nonlinear function of the amplitude of A_1 and presents a maximum for a specific value of $|A_1|$ and, thus, for a specific input impedance Z_{IN}. Therefore, to calculate the resonator impedance that obtains maximum oscillator power, we only have to plot the analytical expression of the oscillator resonator power and the maximum position can thus be determined. For this value, the correspondent input reflection coefficient can be calculated from (47) (Figure 13). Once

the optimum input impedance is obtained (Z_{IN}), the optimum resonator impedance (Z_{RES}) would be calculated to fulfill the oscillation steady-state condition through

$$Z_{RES}(\omega_0) = -Z_{IN}(A_0, \omega_0). \quad (52)$$

A more detailed description of this method can be found in [37], where results of the application of this procedure to design HBT-based 5-GHz free-running oscillators are shown.

The procedure outlined here provides for a nonlinear analytic aid to oscillator design, based on a limited set of measured behavioral parameters, to obtain the optimum values for Z_T and Z_{RES} in real time. The last step of the design procedure will be the synthesis and optimization of the matching networks to achieve the performance compatible with Z_T and Z_{RES}. For this specific purpose, simulation aids such as HB or *S*-parameters may be extremely helpful.

A validation of the solution obtained using this procedure to design a HBT-based 5-GHz free-running oscillator is shown in Table 2. In this example, the optimum values for Z_T and Z_{RES} were obtained from the analytical design procedure and used analytically or numerically (in HB simulations with the *X*-parameters transistor model) to compute the oscillator performance. Table 2 shows the comparison of the analytically predicted performance and the simulated (HB, oscillator mode) one. Note that the main advantage of using this analytical design method is to quickly obtain a valid solution; i.e., the optimum values for Z_T and Z_{RES} compatible with the oscillator desired performance. In this way, the computed behavioral parameters can be used in the analytical expressions to provide design guidance toward an optimum solution, making more efficient use of the time spent on design.

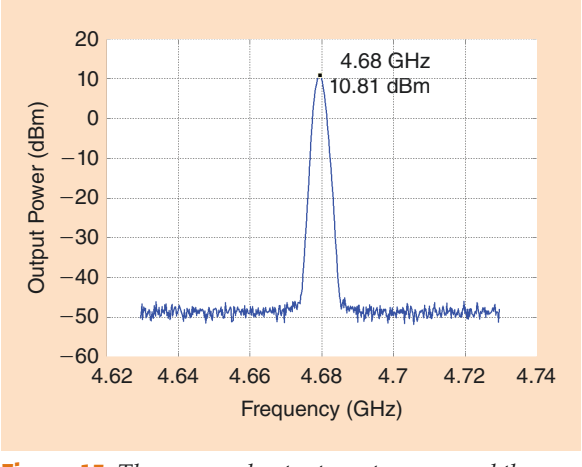

Figure 15. *The measured output spectrum around the fundamental frequency component of the manufactured 5-GHz HBT-based oscillator circuit.*

Hence, it enables the development of a similar set of algebraically defined design aids, as in the case of *S*-parameters, but also valid in the large-signal regime.

This design method does not include any approximations outside those considered in the behavioral transistor description. Hence, the higher the Q of the resonator, the less impact this approximation will have, since the role of harmonics is less important. In addition, spurious oscillations are also less probable. If further analysis were required, e.g., due to a low Q, the oscillator designed through this method could be later implemented in a CAD simulator and analyzed for stability using some of the proposed methods based on numerical simulations [42]. Note that an additional rigorous stability analysis of the obtained steady-state solution may also be necessary using numerical pole-zero identification or Nyquist criterion.

The designed oscillator prototype and measured response are shown in Figures 14 and 15, respectively. The results are within the tolerance of the fabrication process, substrate, and discrete components [37].

Conclusions

Exploiting mathematical formulations of nonlinear behavior defined in the frequency domain, analytical design aids have been formulated, similar to those developed from *S*-parameters, that can be used to guide the nonlinear circuit design flow. To date, the formulations derived have focused on predicting performance in terms of varying the fundamental load impedance. However, it is envisaged that additional formulations will emerge that can also consider harmonic source and load terminations.

Acknowledgments

We would like to thank Alejandro Rodríguez-Testera and Orentino Mojón Ojea for their contributions. This work has been supported by Projects TEC2011-28683-C02-01 and TEC2011-29264-C03-03 of the Spanish National Board of Scientific and Technology Research, the European Regional Development Funds, and the Galician Regional Government for funding the Atlantic Research Center for Information and Communication Technologies (AtlantTIC).

References

[1] D. M. Pozar, *Microwave Engineering*. New York: Wiley, 1998.
[2] G. González, *Microwave Transistor Amplifiers: Analysis and Design*. Englewood Cliffs, NJ: Prentice Hall, 1996.
[3] I. Angelov, L. Bengtsson, and M. Garcia, "Extensions of the chalmers nonlinear HEMT and MESFET model," *IEEE Trans. Microwave Theory Tech.*, vol. 46, no. 10, pp. 1664–1674, Oct. 1996.

[4] T. Gasseling, "Compact transistor models: The roadmap to first pass amplifier design success," *Microwave J.*, vol. 55, no. 3, p. 74, Mar. 2012.
[5] C. McAndrew, "VBIC95, the vertical bipolar intercompany model," *IEEE J. Solid-State C.*, vol. 13, no. 10, pp. 1476–1482, 1996.
[6] S. C. Cripps, *RF Power Amplifiers for Wireless Communications*. Norwood, MA: Artech House, 2006.
[7] P. J. Tasker, "Practical waveform engineering," *IEEE Microwave Mag.*, vol. 10, pp. 65–76, Dec. 2009.
[8] D. E. Root, "Future device modeling trends," *IEEE Microwave Mag.*, vol. 13, no. 7, pp. 45–59, Nov./Dec. 2012.
[9] I. Angelov, M. Thorsell, K. Andersson, N. Rorsman, and H. Zirath, "Recent results on using LSVNA for compact modeling of GaN FET devices," in *Proc. IEEE Int. Microwave Symp. Workshop: Device Model Extraction Large-Signal Measurements*, Montreal, QC, Canada, June 2012.
[10] P. J. Tasker and J. Benedikt, "Waveform inspired models and the harmonic balance emulator," *IEEE Microwave Mag.*, vol. 12, no. 2, pp. 38–54, Apr. 2011.
[11] D. M. Snider, "Theoretical analysis and experimental confirmation of the optimally loaded and over-driven RF power amplifier," *IEEE Trans. Electron Devices*, vol. 14, no. 12, pp. 851–857, Dec. 1967.
[12] P. Wright, A. Sheikh, C. Roff, P. J. Tasker, and J. Benedikt, "Highly efficient operation modes in GaN power transistors delivering upwards," in *MTT-S Int. Microwave Symp. Dig.*, Atlanta, GA, June 2008, pp. 1147–1150.
[13] V. Carrubba, A. Clarke, M. Akmal, J. Lees, J. Benedikt, P. Tasker, and S. Cripps, "On the extension of the continuous class-F mode power amplifier," *IEEE Trans. Theory Tech.*, vol. 59, no. 5, pp. 1294–1303, 2011.
[14] V. Carrubba, M. Akmal, R. Quay, J. Lees, J. Benedikt, S. C. Cripps, and P. J. Tasker, "The continuous inverse class-F mode with resistive second-harmonic impedance," *IEEE Trans. Theory Tech.*, vol. 60, no. 6, pp. 1928–1936, 2012.
[15] J. Verspecht, "Describing functions can better model hard nonlinearities in the frequency domain than the volterra theory," Ph.D. dissertation, Dept. ELEC, Vrije Univ., Brussels, Belgium, 1995.
[16] F. Verbeyst and M. V. Bossche, "VIOMAP, the *S*-parameter equivalent for weakly nonlinear RF and microwave devices," in *IEEE MTT-S Int. Microwave Symp. Dig.*, May 1994.
[17] D. E. Root, J. Verspecht, D. Sharrit, J. Wood, and A. Cognata, "Broad-band poly-harmonic distortion (PHD) behavioral models from fast automated simulations and large-signal vectorial network measurements," *IEEE Trans. Microwave Theory Tech.*, vol. 53, no. 11, pp. 3656–3664, Nov. 2005.
[18] J. Verspecht and D. E. Root, "Polyharmonic distortion modeling," *IEEE Microwave Mag.*, vol. 7, pp. 44–57, June 2006.
[19] D. E. Root, J. Horn, L. Betts, C. Gillease, and J. Verspecht, "*X*-parameters: The new paradigm for measurement, modeling, and design of nonlinear RF and microwave components," *Microwave Eng. Europe*, pp. 16–21, Dec. 2008.
[20] D. Root, J. Verspecht, J. Horn, and M. Marcu, *X-Parameters. Characterization, Modeling, and Design of Nonlinear RF and Microwave Components*. Cambridge, U.K.: Cambridge Univ. Press, 2013.
[21] M. Myslinski, F. Verbeyst, M. V. Bossche, and D. Schreurs, "*S*-functions behavioral model order reduction based on narrowband modulated large-signal network analyzer measurements," in *Proc. 75th Microwave Measurements Conf. (ARFTG)*, May 2010, pp. 1–6.
[22] H. Qi, J. Benedikt, and P. J. Tasker, "Nonlinear data utilization: From direct data lookup to behavioral modeling," *IEEE Trans. Microwave Theory Tech.*, vol. 57, no. 6, pp. 1425–1432, June 2009.
[23] S. Woodington, T. Williams, H. Qi, D. Williams, L. Pattison, A. Patterson, J. Lees, J. Benedikt, and P. J. Tasker, "A novel measurement based method enabling rapid extraction of a RF waveform look-up table based behavioral model," in *IEEE MTT-S Int. Microwave Symp. Dig.*, June 2008, pp. 1453–1456.
[24] C. Baylis, R. J. Marks II, J. Martin, H. Miller, and M. Moldovan, "Going Nonlinear," *IEEE Microwave Mag.*, vol. 12, no. 2, pp. 55–64, Apr. 2011.
[25] A. M. Peláez-Pérez, A. Rodríguez-Testera, O. Mojón, M. Fernández-Barciela, P. J. Tasker, and J. I. Alonso, "Utilization and validation of HBT nonlinear frequency domain behavioral models in the design and simulation of oscillator circuits," in *Proc. European Microwave Conf. (EuMC)*, 2010, pp. 481–484.
[26] Y. Wang, D. Sira, T. Nielsen, O. Jensen, and T. Larsen, "On wafer *X*-parameter based modeling of a switching cascode power amplifier," in *Proc. NORCHIP*, 2011, pp. 1–4.
[27] J. Horn, J. Verspecht, D. Gunyan, L. Betts, D. Root, and J. Eriksson, "*X*-parameter measurement and simulation of a gsm handset amplifier," in *Proc. European Microwave Integrated Circuit Conf.*, 2008, pp. 135–138.
[28] J. Cai and T. Brazil, "*X*-parameter-based frequency doubler design," in *Proc. 42nd European Microwave Conf.*, 2012, pp. 1174–1177.
[29] A. Rodriguez-Testera, O. Mojón, A. Boaventura, M. Fernandez-Barciela, N. B. Carvalho, M. V. Bossche, and G. Pailloncy, "Diode power detector *X*-parameters model extraction using LSNA-based measurement system," *Electron. Lett.*, vol. 49, no. 3, pp. 196–198, Jan. 2013.
[30] Agilent. [Online]. Available: http://www.agilent.com
[31] AWR Corporation. [Online]. Available: http://www.awrcorp.com/
[32] A. Pelaez-Perez, S. Woodington, M. Fernandez-Barciela, P. Tasker, and J. Alonso, "Application of an NVNA-Based system and load-independent *X*-parameters in analytical circuit design assisted by an experimental search algorithm," *IEEE Trans. Microwave Theory Tech.*, vol. 61, no. 1, pp. 581–586, 2013.
[33] A. M. Pelaez-Perez, J. I. Alonso, M. Fernandez-Barciela, A. Rodriguez-Testera, P. J. Tasker, and S. Woodington, "Experimental verification of analytical design equations based on *X*-parameters for predicting role of series feedback," in *Proc. European Microwave Integrated Circuits Conf.*, 2011, pp. 148–151.
[34] R. W. Jackson, "Comments on Criteria for the onset of oscillation in microwave circuits," *IEEE Trans. Microwave Theory Tech.*, vol. 40, no. 9, pp. 1850–1851, 1992.
[35] G. Simpson, J. Horn, D. Gunyan, and D. E. Root, "Load-pull + NVNA = enhanced *X*-parameters for PA designs with high mismatch and technology-independent large-signal device models," in *Proc. IEEE ARFTG Conf.*, 2008, pp. 88–91.
[36] R. S. Saini, S. W. J. Lees, J. Benedikt, and P. J. Tasker, "An intelligence driven active load-pull system," in *Proc 75th Microwave Measurements Conf. (ARFTG)*, 2010, pp. 1–4.
[37] A. Pelaez-Perez, S. Woodington, M. Fernandez-Barciela, P. Tasker, and J. Alonso, "Large-signal oscillator design utilizing analytical *X*-parameters closed-form expressions," *IEEE Trans. Microwave Theory Tech.*, vol. 60, no. 10, pp. 3126–3136, 2012.
[38] M. Pelaez-Perez, S. Woodington, J. I. Alonso, M. Fernandez-Barciela, and P. J. Tasker, "*X*-parameters based closed-form expressions for evaluating power dependent fundamental negative and positive real impedance boundaries in oscillator design," *IET Microwaves, Antennas Propagat. J.*, vol. 6, no. 8, pp. 835–840, Apr. 2012.
[39] A. B. Carlson, *Communications systems*. New York: McGraw-Hill, 1986.
[40] A. Suárez, *Analysis and Design of Autonomous Microwave Circuits*. Hoboken, NJ: Wiley, 2009.
[41] G. González, *Foundations of Oscillator Circuit Design*. Norwood, MA: Artech House, 2007, pp. 251–350.
[42] S. Sancho, F. Ramírez, and A. Suárez, "General stabilization techniques for microwave oscillators," *IEEE Microwave Wireless Compon. Lett.*, vol. 15, no. 12, pp. 868–870, Dec. 2005.